Utility of Imaging Spectrometry for Lithologic Mapping in Greenland

*Benoit Rivard** and *Raymond E. Arvidson*
McDonnell Center for the Space Sciences, Department of Earth and Planetary Sciences, Washington University, St. Louis, MO 63130

ABSTRACT: Landsat Thematic Mapper (TM) multispectral image data and field-based spectral reflectance measurements for a portion of the island of Storo, southwestern Greenland, were used to evaluate the potential of imaging spectrometry for lithologic mapping in arctic terrains. TM data allow mapping of tundra vegetation that typically covers moraines at lower elevations, and lichen-covered bedrock exposed at higher elevations. However, the ubiquitous lichen cover, combined with the limited spectral and radiometric capabilities of TM, severely hamper mapping of the amphibolite, anorthosite, gneiss, and granite outcrops on the island. Diagnostic mineral signatures can be discerned from high spectral and radiometric resolution observations, because lichen cover is patchy at mineral and outcrop scales. Results imply that high resolution imaging spectrometer data (e.g., from the HIRIS sensor to fly on the Earth Observing System), detailed field work, and application of subpixel mixing models will dramatically improve the ability to identify and map bedrock in similar terrains.

INTRODUCTION

GEOLOGICAL FIELD WORK IN THE ARCTIC IS EXPENSIVE, logistically difficult, and the field season is relatively short. For these reasons, and because of the importance of the Greenland and Canadian Shields for understanding crustal processes that operated in early Earth history, we initiated a pilot project to investigate the potential use of imaging spectrometry for lithologic mapping in the Archean terranes of southwestern Greenland.

Imaging spectrometry entails simultaneous acquisition of high-quality images in narrow spectral bands (Goetz *et al.*, 1985). The resultant data allow both spatial and spectral domains to be analyzed with high spectral and radiometric resolutions. Spectral resolution is related to the extent to which fine spectral detail can be discerned which is dependent on spectral contrast. For example, very narrow bands spaced 10 nm apart are required to sample properly an absorption feature with a width of approximately 20 nm (Nyquist theorem), assuming the system has enough radiometric resolution to detect the feature. Radiometric resolution is related to the ability to detect subtle reflectance differences and is governed by signal-to-noise constraints and the encoding scheme (e.g., Elachi, 1987). The High Resolution Imaging Spectrometer (HIRIS) planned for the Earth Observing System in the late 1990s will allow high spectral and radiometric resolution data to be obtained over large parts of the Earth's surface (Table 1 and Goetz *et al.* (1987)). Design of HIRIS was driven in part by the requirement to sample properly the charge transfer, electronic transition, and narrow vibrational absorption features that are diagnostic of mineralogy in the visible and reflected infrared wavelength interval. It is expected that HIRIS will enable a new era of lithologic mapping from remote sensing for regions with some exposed bedrock (Goetz *et al.*, 1985; 1987).

The presence of tundra vegetation and lichen cover in arctic terrains compromises the ability to map reflectance signatures diagnostic of mineralogy from imaging spectrometry data. We evaluated the magnitude of this problem by (a) utilizing Landsat TM data as a low spectral and radiometric resolution imaging spectrometer for selected areas in southwestern Greenland (Figure 1), and (b) evaluating additional information that could be obtained from higher spectral and radiometric resolution data by acquiring and analyzing field spectrometer observations for the same areas. Field work focused on understanding the patterns seen in the TM data was also conducted, and relevant samples were collected and examined in hand specimen and thin section. Field work was conducted in June, 1988.

ANALYSIS OF TRAVERSE AND GRID SITES

The islands Qilangarssuit, Storo, Sadelo, Bjorneoen, and a region outside of Nuuk were the sites of our field studies (Figure 1). For this paper, we focus on a portion of the island of Storo. Storo is east of Godthabsfjord and is characterized by steep topography, extensive lichen-covered bedrock exposures at intermediate elevations, and perennial snowfields at highest elevations. The lowlands are dominated by tundra vegetation that typically grows on moraines. Lithologic units exposed include Nuuk and Amitsoq gneisses, anorthosites, granites, and Malene amphibolite rocks. Thus, Storo offers a wide variety of vegetative cover and lithology.

To characterize this diversity, five field traverses were conducted, a grid (60 m by 60 m) was laid out where materials were characterized at 5-metre intervals, and several dozen samples were collected. The grid site is on a region previously mapped as moraine (Figure 1). For the grid site we found that 70 percent of the surface consists of tundra vegetation growing over moraine deposits, and 30 percent consists of Nuuk gneiss outcrops. The areal extent of lichen cover on the outcrops is approximately 80 percent. Thus, for the grid site, bare rock is exposed over approximately 6 percent of the surface area. The bare rock is relatively unweathered and is exposed in discrete patches that range from centimetres to metres in width. This result is typical of such sites, based on our field traverse observations on Storo and elsewhere. We also found that lichen covers approximately 80 percent of the outcrops for areas above the tundra vegetation. The remaining 20 percent consists of patches of relatively unweathered rock.

ANALYSIS OF LANDSAT THEMATIC MAPPER DATA

In this section, we focus on the generation and analyses of products that illustrate the utility of TM observations for lithologic mapping on Storo. Under the relatively clear atmospheric conditions during TM data acquisition, the influence of the atmosphere on the surface radiance measured by TM in the visible

*Presently with the Earth Observation Laboratory, Institute for Space and Terrestrial Science, York University, North York, Ontario M3J 3K1, Canada.

PHOTOGRAMMETRIC ENGINEERING & REMOTE SENSING,
Vol. 58, No. 7, July 1992, pp. 945–949.

0099-1112/92/5807-945$03.00/0

TABLE 1. FUNCTIONAL CHARACTERISTICS OF LANDSAT THEMATIC MAPPER (TM), DAEDALUS SPECTROMETER, AND HIGH RESOLUTION IMAGING SPECTROMETER (HIRIS).

Instrument	Pixel Width (m)	Image Dimension (km)	Spectral Bands	Encoding (bits/pixel)
Thematic Mapper	30	185	6 bands (0.4 to 2.4 μm) (see Figure 2 for band locations.)	8
Daedalus AA440 Spectrafax Spectrometer	3 cm at 1 m Height	N/A	288 bands (0.45 to 2.4 μm) Band spacing ranges from 9 nm at 0.45 μm to 40 nm at 1.3 μm	10
High Resolution Imaging Spectrometer: (EOS instrument)	30	30	192 bands (0.4 to 2.5 μm) Band spacing approximately 10 nm	12

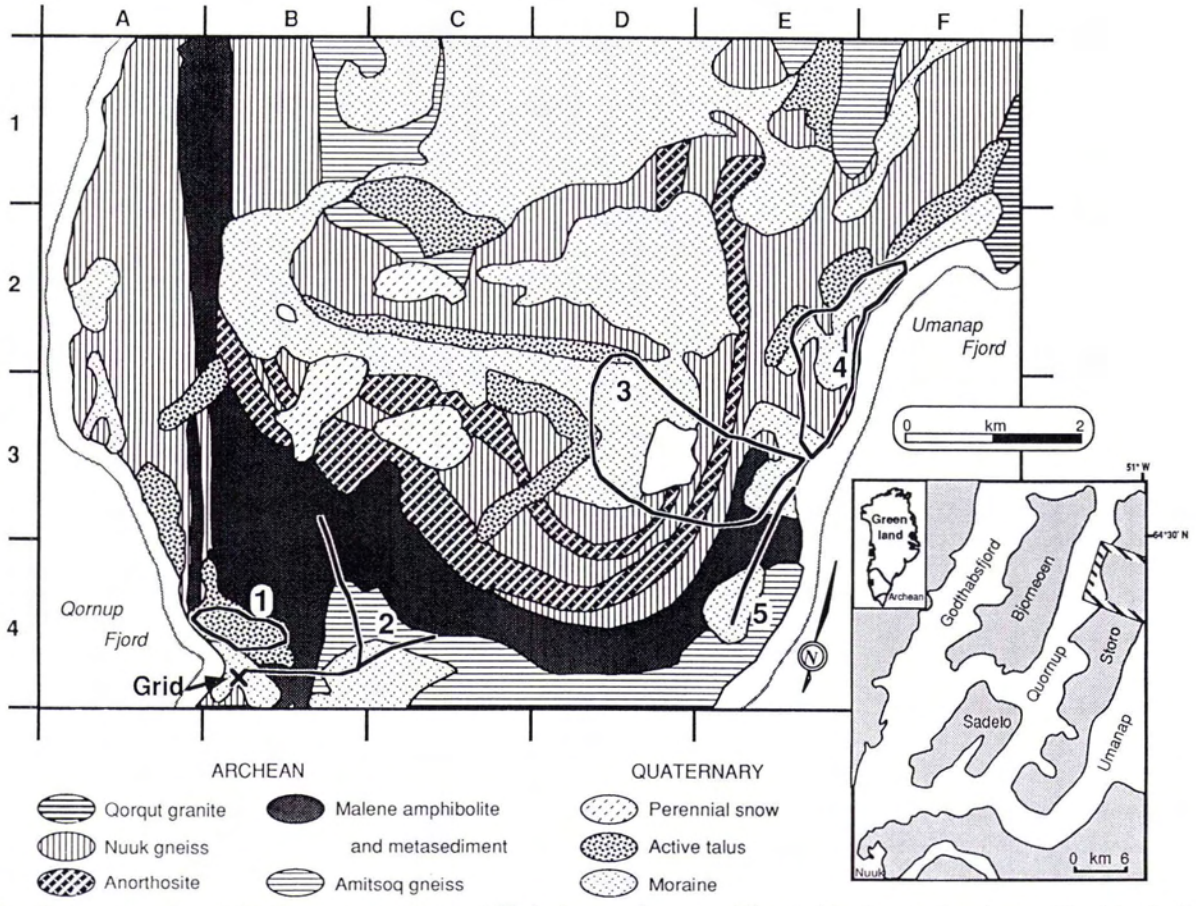

FIG. 1. Location map of the Storo study area and lithologic map for area delineated by box on inset map. The island of Qilangarssuit was also included in our field work. It is located about 30 km south of Nuuk. Geologic units after the 1:100 000 Qorqut 64V1 sheet (Geological Survey of Greenland, 1984). Five traverses (numbered) and a grid site are also shown.

and reflected infrared can be expressed as an additive increase in the signal due to light scattered directly by the atmosphere to TM, and a multiplicative effect due to attenuation of the surface radiance during atmospheric transit. As a first step, we generated images with lightness values in proportion to radiance received on the sensors, using the standard calibration values supplied with the TM data. Our intent was to evaluate the extent to which various lithologic units could be discerned using TM data, not to extract absolute surface radiances or reflectances. The ability to discriminate units is not strongly influenced by the presence of the atmospheric term, as long as the atmosphere is fairly clear and spatially invariant. Careful examination of the data over water in the fjords and in deep lakes shows that the atmosphere was, in fact, clear over the entire scene and that there were no clouds. Thus, we were able to pursue standard enhancement techniques such as linear contrast stretches, band ratios, generation of color composites, and nearest-neighbor and Gaussian classifiers (Richards, 1986) to explore the extent to which TM data portray lithologic variations. Whereas the various standard enhancements were investigated, only the color composite is used in this discussion.

Plate 1 is a color composite covering the traverse and grid

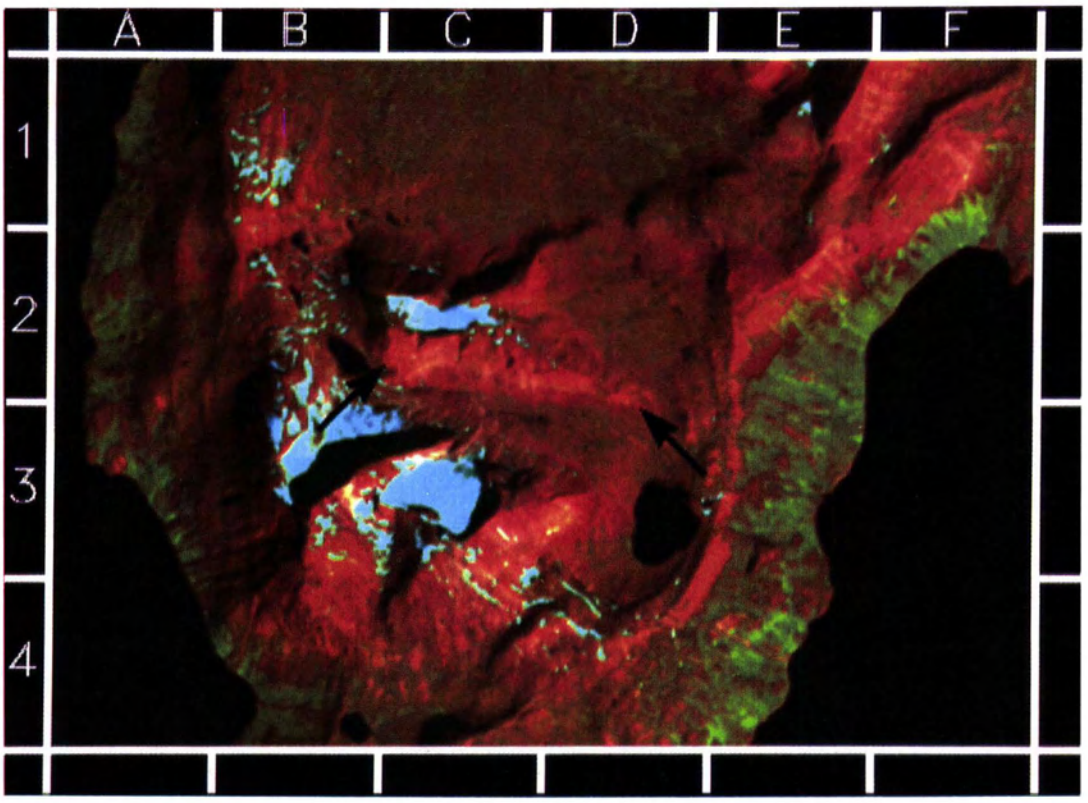

PLATE 1.TM color composite for the same part of Storo as shown in Figure 1. Bands 1, 4, 7 were assigned respectively to blue, green, and red components. See Figure 2 for band wavelength locations. Arrows at C2, D2 delineate ends of E-W trending Nuuk gneiss and talus units discussed in text. TM scene I.D.Y51236 14085X0, acquired on 20 July 1987, with a solar incidence angle of 46°.

sites in Storo. TM bands 1, 4, and 7 are assigned to blue, green, and red components, respectively. We found that the 1,4,7 color composite portrays the majority of material types that can be discerned using composites, ratios, and automatic classifiers. In the composite, the tundra vegetation that covers moraine deposits on the lowlands has a relatively high band 4 lightness and appears green, a result consistent with reflectance from green, leafy vegetation (e.g., Knipling, 1970). The areal distribution of green areas in the TM composite suggests that moraine is more widely distributed than shown on the existing geologic map (e.g., at E2 to E4 and F2 to F4 in Figure 1), an interpretation that we verified in the field. Arctic willow and birch are replaced by mosses at elevations higher than approximately 200 m. This change in vegetation type apparently causes the change from green colors at lower elevations to brown-green colors at higher elevations. The brown, orange, and yellow colors at higher elevations are associated with lichen-covered bedrock. The color patterns are consistent with rock and lichen reflectance signatures, both of which typically increase with increasing wavelength in the visible and reflected infrared (e.g., Hunt, 1977; Ager and Milton, 1987). Finally, cyan-colored snow fields dominate the highest elevations.

We found that identifying and mapping rock types from the TM was impossible to do for regions covered by tundra vegetation and difficult to do for lichen-covered bedrock areas. For example, note the lack of correspondence between the TM product and the geologic map for the green-colored (i.e., tundra vegetation) regions. Also, note the general lack of correlation between colors on the TM product and bedrock types for regions above the tundra vegetation. There is some lithologic information portrayed, but detailed field work is necessary to understand lithologic controls on the various orange and brown colors evident in the composite. For example, the bright orange color of the Nuuk outcrops at C2 to D2 in Plate 1 is due to the exposure of relatively smooth, steep outcrops kept free of lichen by spalling. Lichen-covered talus just to the south of these outcrops is dark brown, because of the lichen and the rough nature of the deposit, i.e., it casts shadows. This dark brown color is also characteristic of lichen-covered outcrops of Malene amphibolites at B4. For the Malene rocks, the color is controlled by lichen and the intrinsically dark reflectance of the amphibolite exposures.

Results suggest that TM-based products could be used as first-order products to distinguish regions with tundra vegetation, as opposed to lichen-covered rock exposures. Detailed lithologic mapping would require a significant amount of field work to unravel ambiguities. We postulate that the inability to use TM to discriminate among rock types is due to the limited spectral (six broad bands) and radiometric (8-bit encoding) resolutions inherent to the instrument. The high degree of undersampling of vegetation and rock spectral features is well known for TM data (e.g., Elachi, 1987; Sultan *et al.*, 1987). As to radiometric resolution, we note that because of the low solar incidence angle (46°), the data only occupy the lower 50 percent of the 8-bit dynamic range. This coarse radiometric granularity must also contribute to the inability to distinguish among rock types in this area using TM data.

FIELD SPECTROMETER OBSERVATIONS

In this section we consider the utility of high radiometric and spectral resolution observations for resolving the lithologic ambiguities evident in TM data. Our approach was to acquire relatively high resolution spectral reflectance data using a field spectrometer (Table 1) to define the inherent lithologic infor-

mation available at fine scales (centimetres). Unfortunately, logistical difficulties precluded use of the instrument on Storo. Data were collected in the field for numerous surfaces at the Qilangarssuit site (Figure 1) and samples from all sites were collected and measured in the laboratory. Based on our field observations, the characteristic tundra vegetation, lichen, and rock exposures are similar at all of our study sites and vary primarily with elevation. Thus, we feel comfortable using spectral data from Qilangarssuit to define centimetre-scale information for all study areas, including the Storo site.

Measurements were made with the spectrometer head approximately 1 metre from the surface, using an internal tungsten halogen light source. The spectrometer field of view was approximately 5 cm^2 and the observation phase angle was a few degrees. The instrument spectral and radiometric resolutions are given in Table 1. Raw data were smoothed using a five-band arithmetic moving average. The smoothed spectral radiance data for given materials were converted to radiance coefficients by dividing the radiance of the measured surface by the radiance of a unit lightness Lambertian Spectrahalon standard surface identically illuminated (Hapke, 1981). Detailed examination of the smoothed spectra suggests that known absorption features with full-width, half-maximum absorptions of 60 to 80 nm are properly sampled if they have a depth of at least several percent relative to the continuum.

Figure 2A displays spectra of snow, tundra vegetation, and the spectrum of clear, deep water. As noted in the last section, these surface materials, along with lichen-covered bedrock and rock exposures, encompass most of the variety observed on Storo. The clear water spectrum has highest radiance coefficient values in the blue-green wavelength range. Snow provides some return in the blue range (0.4 to 0.5 μm), displays a peak near 1.0 μm, and has a low reflectance in the infrared. The tundra vegetation sample consists of mosses and pieces of leafy bushes. The tundra spectrum is typical of green plants, characterized by water absorption features at 1.4 and 1.9 μm and a broad, high plateau in the 0.9 to 1.3 μm range due to scattering from leaves. Results imply that the reflectance of snow will dominate in TM bands 1 and 4, whereas vegetation reflectance will be highest in band 4. These results are consistent with the color trends observed in Plate 1. Spectra of lichen-free granodiorite, tonalite, and amphibolite natural rock surfaces are shown on Figure 2B. Based on thin section and hand specimen examination, the amphibolite sample M1 contains equal amounts of actinolite and plagioclase, and about 1 percent accessory minerals. M2 contains about 2/3 actinolite, 1/3 plagioclase, and 1 percent accessories minerals, including epidote. The presence of abundant actinolite with charge-transfer, electronic-transition, and vibration-related absorptions causes the low overall reflectance (Hunt and Salisbury, 1973). Narrow actinolite-related vibrational absorption features between 2.30 and 2.35 μm are apparent, although there is not enough resolution to sample fine structure evident in detailed laboratory spectra for actinolites (e.g., Clark *et al.*, 1990). The granodiorite (G1) consists of about 30 percent each of plagioclase feldspar, hornblende, epidote, and 10 percent quartz. The tonalite (G2) consists of about 2/3 plagioclase and 1/3 epidote, biotite, and hornblende. The granodiorite and tonalite reflectances are higher than the amphibolite reflectances because of the lower abundance of mafic minerals. The presence of biotite in G2 probably causes the lower overall reflectance as compared to G1. The absorption feature at 1.9 μm in G1 is consistent with the presence of molecular water, probably as fluid inclusions in quartz (Hunt and Salisbury, 1973). Epidote has vibrational absorptions at 2.25 and 2.34 μm (Clark *et al.*, 1990). These features, together with features related to hornblende explain the G1 and G2 spectra near 2.2 to 2.4 μm. Thus, the data shown in Figure 2B demonstrate that the rocks common to southwestern Greenland have spectra with features that are diagnostic of mineralogy.

The spectra on Figures 2C and 2D characterize the spectral features diagnostic of black crustose and foliose lichens that dominate the study sites. The visible color of lichens is due to chlorophyll absorption and to strong absorption in the ultraviolet due to usnic acid (Knipling, 1970; Longton, 1988), thus explaining the low reflectances at shorter wavelengths. The absorption features at 1.4 and 1.9 μm are due to the presence of water, whereas features located near 2.1 and 2.3 μm are related to cellulose, a major constituent of the cells forming the walls of fungi (Hale, 1983).

Overall, the spectra of lichens are distinct in shape from that of underlying bedrock. This result is generally consistent with previous spectral studies of lichens by Ager and Milton (1987)

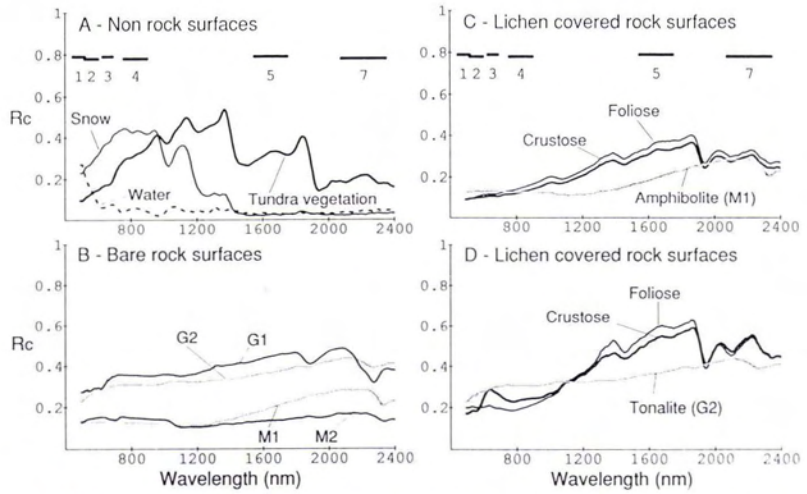

FIG. 2. Radiance coefficient spectra acquired in the field for snow, water, and tundra vegetation are shown in A. Graph B shows spectra of lichen-free rocks, as follows: M1, M2 are Malene amphibolites; G1 is a Nuuk granodiorite; G2 is a coarse-grained Amitsoq tonalite. Graphs C and D show spectra for lichen-covered M1 and G2 surfaces, respectively. Lichen types are labeled. Also shown for comparison in C and D are the M1 and G2 rock spectra from graph B. Bandpasses for Landsat TM bands 1-5 and 7 are shown as thick black lines on the top graphs. Note that TM band widths are much too wide and the spacing is too irregular to sample the spectra properly.

and Satterwhite *et al.* (1985). However, bedrock control of lichen signatures is also evident in the data and is explained by rock and mineral exposures at millimetre scales. For example, note that the lichen on M1 has a lower reflectance and more subdued absorption features than the lichen on G2. Based on microscopic examination, 20 to 40 percent of the area included in the reflectance measurement for the crustose lichen on M1 actually consists of bare actinolite grains that stand above surrounding plagioclase crystals (Rivard, 1990). Approximately 20 percent of the area consists of actinolite exposures for the foliose lichen spectrum acquired on M1. For G2, approximately 20 percent of rock is exposed for the area used to acquire the crustose lichen spectrum, whereas the foliose lichen on the tonalite completely obscures the underlying rock. Clearly, the exposure of dark actinolite crystals lowers the "lichen" reflectances on M1. Likewise, the exposure of 20 percent rock for the G2 crustose lichen spectrum explains the difference between this spectrum and the G2 foliose spectrum, including the rock and crustose spectra contrast reversal at 1.1 μm, relative to the foliose spectrum. Thus, even for lichen-covered surfaces, rock contributes to reflectance signatures. However, it would be difficult to identify the lichen and rock contributions uniquely via specific absorption features with the spectral resolution inherent for the data shown in Figure 2. This difficulty is exacerbated by the overlap of the 2.2 to 2.4 μm diagnostic vibrational features on rocks with cellulose-related absorptions for the lichen.

IMPLICATIONS FOR THE USE OF IMAGING SPECTROMETRY FOR ARCTIC TERRAINS

HIRIS spatial resolution will be similar to the resolution of the TM data. On the other hand, we note that the spectral resolution will be much better than TM (192 narrow bands versus 6 broad bands over the same wavelength interval; see Table 1), and 6 to 9 times better than the smoothed field spectrometer data shown in Figure 2. The radiometric accuracy will be 16 times better than TM, and 4 times better than our field spectrometer, based on the encoding schemes (Table 1). Furthermore, other EOS instruments will be acquiring data on atmospheric properties at the same time that HIRIS is imaging the surface. Thus, true surface reflectance values will be extractable, in addition to being able to generate products such as the composite shown in Plate 1.

Given that HIRIS spectral and radiometric resolution will exceed those for the spectra shown in Figure 2, and given that lichen is patchy over both mineral grain and outcrop scales, we conclude that HIRIS will be a powerful tool to isolate, identify, and map rock types in southwestern Greenland and similar areas. For example, as noted, high-resolution laboratory spectra of minerals characteristic of the Malene amphibolites, Nuuk granodiorite, and Amitsoq tonalite show diagnostic fine-scale absorptions not captured in our field spectrometer data (e.g., Clark *et al.*, 1990). HIRIS will have the resolution to sample properly much of the fine-scale spectral information and, presumably, be able to separate rock and lichen-related spectral features in the 2.2- to 2.4-μm region. However, it is also clear that extensive field work, including high-resolution field spectrometry, will be needed to interpret HIRIS data, because the typical HIRIS spectrum will be a sub-pixel mixture of tundra vegetation, lichen, and rock spectral endmembers.

ACKNOWLEDGMENTS

This work was supported by the NASA Geology Program under Grant NAGW 1358 to Washington University and by an FCAR Graduate Fellowship to BR, awarded by the government of Quebec. Our thanks are extended to Robert Dymek, E. O'Leary, Kent Swanson, and Brian Curtis.

REFERENCES

Ager, C. M., and N. M. Milton, 1987. Spectral reflectance of lichens and their effects on the reflectance of rock substrates: *Geophysics*, Vol. 52, pp. 898-906.

Clark, R. N., T. V. King, M. Klejwa, and G. A. Swayze, 1990. High Spectral resolution reflectance spectroscopy of minerals, *J. Geophys. Res.*, Vol. 95, pp. 12653-12680.

Elachi, C., 1987. *Introduction to the Physics and Techniques of Remote Sensing*, J. Wiley Pub. 413 p.

Geological Survey of Greenland, 1984. 1:100 000 geologic map, Qorqut, sheet 64 V1 South.

Goetz, A. F. H., G. Vane, J. Solomon, and B. Rock, 1985. Imaging spectrometry for Earth remote sensing, *Science*, Vol. 228, pp. 1147-1153.

Goetz, A. F. H., and others, 1987. *High-Resolution Imaging Spectrometer: Science Opportunities for the 1990's*: NASA Instrument panel report, Earth Observing System, Vol. IIc, 74 p..

Hale, M. E., 1983. *Biology of Lichens*, E. Arnold Limited, 495 p..

Hapke, B., 1981. Bidirectional reflectance spectroscopy 1. Theory. *J. Geoph. Res.*, Vol. 86 (B4), pp. 3039-54.

Hunt, G. R., 1977. Spectral signatures of particulate minerals in the visible and near infrared, *Geophysics*, Vol. 42, pp. 501-513.

Hunt, G. R., and J.. Salisbury, 1973. Visible and near-infrared spectra of minerals and rocks: VI. Additional silicates: *Modern Geology*, Vol. 4, pp. 85-106.

Knipling, E. B., 1970. Physical and physiological basis for the reflectance of visible and near-infrared radiation from vegetation: *Rem. Sens. Env.*, Vol. 1, pp. 155-159.

Longton, R. E., 1988. *Biology of Polar Bryophytes and Lichens*: Cambridge University Press.

Richards, J. A., 1986. *Remote Sensing Digital Image Analysis*, Springer-Verlag, 281 p.

Rivard, B., 1990. *Lithologic Mapping in the Southwestern Greenland and Nubian Shields Using Field, Laboratory, and Landsat Thematic Mapper Data*: Ph.D. thesis, Washington University, St.Louis, 225 p..

Satterwhite, M. B., J. P. Henley, and J. M. Carney, 1985. Effects of lichens on the reflectance spectra of granitic rock surfaces: *Rem. Sens. Env.*, Vol. 18, pp. 105-112.

Sultan, M., R. Arvidson, N. Sturchio, and E. Guinness, 1987. Lithologic mapping in arid regions with Landsat thematic mapper, *Geol. Soc. Am. Bull.*, Vol. 99, pp. 748-762.

(Received 1 July 1991; accepted 18 October 1991)